

# Synaptic depression enables neuronal gain control

Jason S. Rothman<sup>1</sup>, Laurence Cathala<sup>1\*</sup>, Volker Steuber<sup>1\*</sup> & R. Angus Silver<sup>1</sup>

To act as computational devices, neurons must perform mathematical operations as they transform synaptic and modulatory input into output firing rate<sup>1</sup>. Experiments and theory indicate that neuronal firing typically represents the sum of synaptic inputs<sup>1–3</sup>, an additive operation, but multiplication of inputs is essential for many computations<sup>1</sup>. Multiplication by a constant produces a change in the slope, or gain, of the input–output relationship, amplifying or scaling down the sensitivity of the neuron to changes in its input. Such gain modulation occurs *in vivo*, during contrast invariance of orientation tuning<sup>4</sup>, attentional scaling<sup>5</sup>, translation-invariant object recognition<sup>6</sup>, auditory processing<sup>7</sup> and coordinate transformations<sup>8,9</sup>. Moreover, theoretical studies highlight the necessity of gain modulation in several of these tasks<sup>9–11</sup>. Although potential cellular mechanisms for gain modulation have been identified, they often rely on membrane noise and require restrictive conditions to work<sup>3,12–18</sup>. Because nonlinear components are used to scale signals in electronics, we examined whether synaptic nonlinearities are involved in neuronal gain modulation. We used synaptic stimulation and the dynamic-clamp technique to investigate gain modulation in granule cells in acute slices of rat cerebellum. Here we show that when excitation is mediated by synapses with short-term depression (STD), neuronal gain is controlled by an inhibitory conductance in a noise-independent manner, allowing driving and modulatory inputs to be multiplied together. The nonlinearity introduced by STD transforms inhibition-mediated additive shifts in the input–output relationship into multiplicative gain changes. When granule cells were driven with bursts of high-frequency mossy fibre input, as observed *in vivo*<sup>19,20</sup>, larger inhibition-mediated gain changes were observed, as expected with greater STD. Simulations of synaptic integration in more complex neocortical neurons suggest that STD-based gain modulation can also operate in neurons with large dendritic trees. Our results establish that neurons receiving depressing excitatory inputs can act as powerful multiplicative devices even when integration of postsynaptic conductances is linear.

The way a neuron transforms signals can be captured by its input–output relationship (Fig. 1a). A modulatory input can change the shape of this relationship, thereby performing a mathematical operation on this transfer function. A shift along the input axis corresponds to an additive operation (+), whereas a change in slope corresponds to a multiplicative operation, or gain change (×). Cerebellar granule cells (GCs) are well suited for studying gain modulation because they have few synaptic inputs. Excitation comes from approximately four mossy fibres (MFs), which can sustain rate-coded signals over a large bandwidth<sup>20</sup> and have STD<sup>19,21</sup>. Inhibition comes from Golgi cells, most of which is mediated by a modulatable tonic GABA<sub>A</sub> (γ-aminobutyric acid subtype A) receptor (GABA<sub>A</sub>) conductance<sup>22</sup>. Because it is difficult to activate multiple inputs independently, and because we wanted to compare real synaptic inputs showing frequency-dependent STD with artificial synaptic inputs without STD, we used dynamic-clamp to study synaptic integration.

GCs are ideal for this because their soma and dendrites form a single electrical compartment, allowing dendritic inputs to be mimicked by somatic conductance injection<sup>13</sup>.

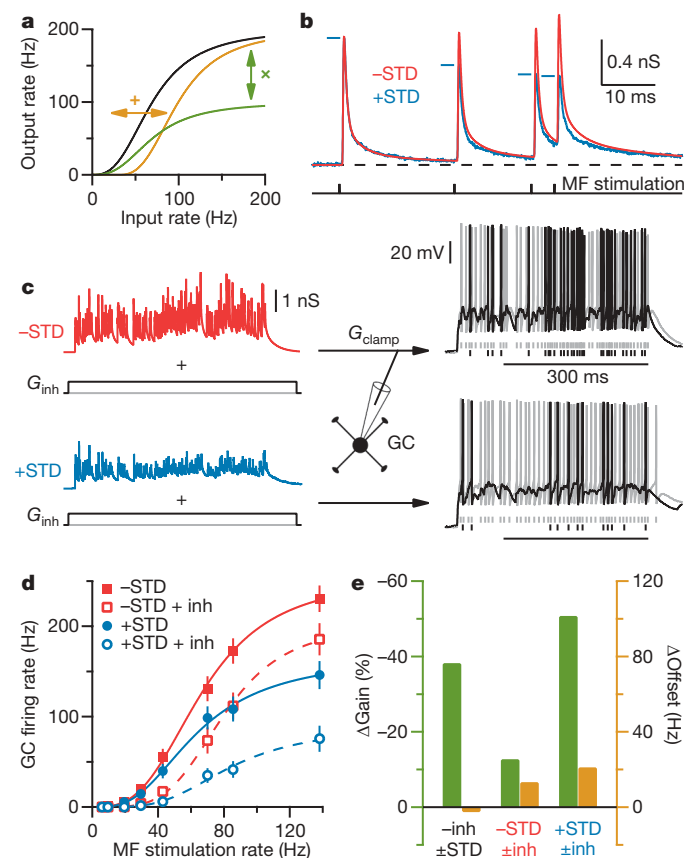


**Figure 1 | Synaptic depression enhances inhibition-mediated gain modulation.** **a**, Hypothetical neuronal input–output relationship before (black) and after multiplicative gain modulation (green, ×) and an additive offset (orange, +). **b**, Averaged AMPAR-mediated synaptic train showing STD (blue trace) in response to Poisson stimulation (black ticks;  $f = 86$  Hz) of single MF inputs; blue ticks show the peak amplitude of the depressing synaptic conductances. The red trace shows the corresponding artificial synaptic train without STD. The black dashed line is the zero conductance level. **c**, The sum of four independent synaptic trains (each  $f = 86$  Hz) with and without STD injected into a GC by means of dynamic clamp ( $G_{\text{clamp}}$ ) with and without tonic inhibition (black and grey, respectively;  $G_{\text{inh}} = 500$  pS). Right vertical ticks indicate spike times. Horizontal bars indicate output rate measurement window.  $V_{\text{rest}} = -79$  mV. **d**, Average input–output relationships ( $n = 9$ ) with and without STD (blue and red, respectively) and tonic inhibition (inh, open and filled symbols, respectively; error bars are  $\pm$ s.e.m.). Lines are fits to a Hill function (equation (5) in Methods; Supplementary Table 1). **e**, Gain (green) and offset (orange) changes due to STD ( $\pm$ STD) and inhibition ( $\pm$ inh) from fits in **d**.

<sup>1</sup>Department of Neuroscience, Physiology and Pharmacology, University College London, Gower Street, London WC1E 6BT, UK.

\*These authors contributed equally to this work.

We measured AMPA ( $\alpha$ -amino-3-hydroxy-5-methyl-4-isoxazole propionic acid) receptor (AMPA)-mediated excitatory postsynaptic currents (EPSCs) from mature GCs at physiological temperature during Poisson-type stimulation of single MFs at different frequencies. These EPSC trains, which showed STD, were then converted to conductance (Fig. 1b, +STD, blue traces throughout). Artificial conductance trains without STD (-STD, red traces throughout) but with identical event timing were constructed by adding a fixed amplitude synaptic conductance waveform at each stimulus time. The effects of STD on synaptic integration were then investigated by injecting the sum of four statistically independent conductance trains with the same mean MF rate into GCs using dynamic-clamp and measuring the mean output firing rate with and without STD (Fig. 1c). The resulting steady-state input–output relationships revealed that STD had an almost purely multiplicative effect under control conditions (Fig. 1d). Multiplicative and additive transformations of the input–output relationship were quantified by fitting the data to Hill-like equations<sup>16</sup> (Fig. 1d, equation (5) in Methods and Supplementary Table 1) and measuring the change in slope (Fig. 1e,  $\Delta$ Gain, green) and the shift in the half maximal response ( $\Delta$ Offset, orange). In the absence of STD, adding a 500 pS tonic inhibitory conductance ( $G_{inh}$ ; Fig. 1c) close to the physiological value ( $438 \pm 93$  pS (mean  $\pm$  s.e.m.);  $n = 10$ ) produced a modest scaling of the input–output relationship together with an additive shift<sup>13</sup> (Fig. 1d, e). In contrast, the same level of inhibition produced a fourfold larger gain change in the input–output relationship when driven with depressing synapses. Moreover, this multiplicative scaling was nearly constant over the entire input range (Supplementary Fig. 1).

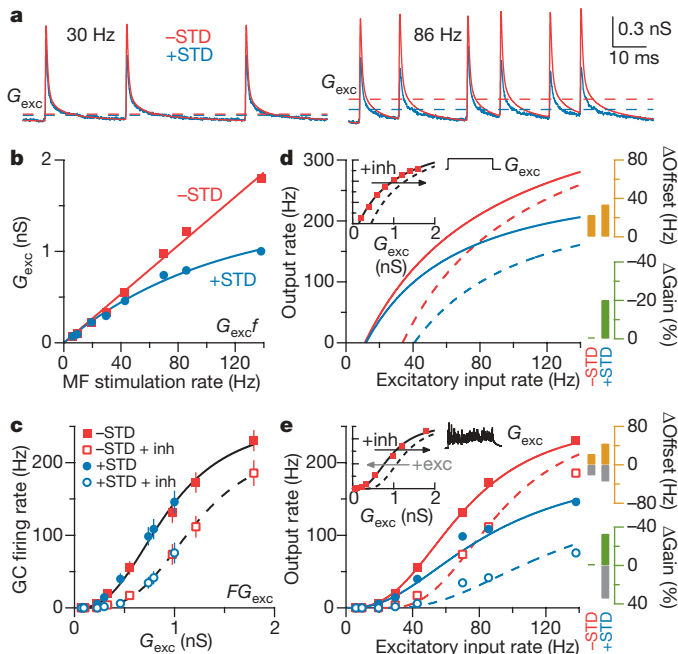


**Figure 2 | Synaptic depression transforms additive shifts into multiplicative gain modulation.** **a**, Average AMPAR-mediated synaptic conductance trains with and without STD (blue and red, respectively) with their time-averaged conductances ( $G_{exc}$ ; dashed lines). **b**,  $G_{exc}$  versus MF rate ( $f$ ) with and without STD. The red line is a linear fit (equation (3), Methods); the blue line is an exponential fit (equation (4)). **c**, Data in Fig. 1d are plotted as output rate ( $F$ ) versus  $G_{exc}$ . Lines are Hill fits (equation (5)) and error bars are  $\pm$  s.e.m. **d**, Predicted input–output relationships computed from  $G_{exc}f$  relationships in **b**, and experimentally measured GC  $FG_{exc}$  relationship generated with noise-free excitatory conductance steps (inset, red squares from Fig. 2b in ref. 13). The solid line in inset is a Hill fit, and the dashed line is the same curve rightward shifted 0.3 nS along the  $G_{exc}$  axis. Bar graphs show changes in gain (green) and offset (orange) due to inhibition with and without STD. **e**, Same as **d**, except control  $FG_{exc}$  data (inset) are from **c** during noisy synaptic excitation. The predicted change in the input–output relationship for STD match the experimental observations (blue symbols). Grey bars show gain and offset changes for a leftward shift of 0.3 nS to simulate excitation.

To understand how STD performs multiplicative gain modulation, we examined the frequency-dependence of the time-averaged excitatory conductances ( $G_{exc}$ ; Fig. 2a, dashed lines). Without STD, the relationship between  $G_{exc}$  and MF input rate ( $f$ ) was linear (Fig. 2b). With STD, it became noticeably sublinear above 40 Hz and could be fit with a saturating exponential function (Fig. 2b). To examine how  $G_{exc}$  was integrated postsynaptically, we plotted the mean GC firing rate ( $F$ ) as a function of  $G_{exc}$ . We found that the  $FG_{exc}$  relationships with and without STD overlaid (Fig. 2c), indicating that  $G_{exc}$  was integrated similarly for both cases. Thus, the nonlinearity between  $f$  and  $G_{exc}$  introduced by STD underlies the enhanced gain modulation.

Because neuronal gain can be altered by synaptic noise<sup>3,13</sup>, we examined how STD transforms GC  $FG_{exc}$  relationships generated with noise-free conductance steps (Fig. 2d, inset<sup>13</sup>) and noisy synaptic conductances (Fig. 2e, inset). Hill equations were used to mimic  $FG_{exc}$  relationships (Fig. 2d, e, insets) whereas linear and exponential functions were used to represent  $G_{exc}f$  relationships (Fig. 2b). These were then combined to predict the input–output relationships. In the absence of STD, additive shifts in the  $FG_{exc}$  relationship produced a purely additive shift in the input–output relationship (Fig. 2d, e), consistent with conductance performing an additive operation when the noise level is constant<sup>2,3</sup>. In contrast, when STD was present, additive shifts in the  $FG_{exc}$  relationship produced robust gain changes in the input–output relationship for both noise-free and noisy excitation (Fig. 2d, e). Indeed, the gain change predicted from purely additive shifts in the  $FG_{exc}$  relationship accounted for most of that observed experimentally (Fig. 2e). This shows that STD transforms linear, additive modulation of the  $FG_{exc}$  relationship into multiplicative gain modulation of the input–output relationship, irrespective of the presence of synaptic noise.

Our experimental results were reproduced in a conductance-based integrate-and-fire model that included short-term synaptic plasticity (Supplementary Fig. 2a, b) confirming the primary role of STD in gain modulation, rather than synaptic noise or other nonlinear synaptic

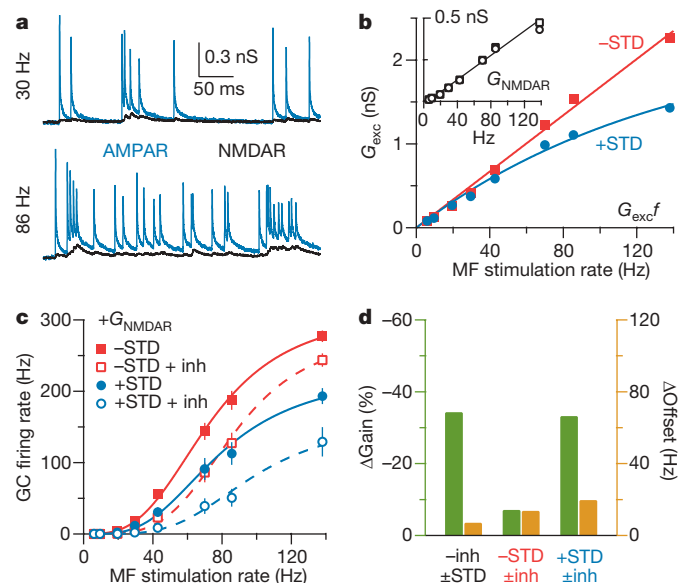


**Figure 3 | Gain modulation in the presence of synaptic NMDAR conductances.** **a**, Average AMPAR (blue) and NMDAR (black) synaptic conductance trains from the same four GCs during Poisson stimulation of individual MF inputs. **b**,  $G_{exc}$  versus MF rate ( $f$ ) for AMPAR + NMDAR components with and without AMPAR STD. Red and blue lines are fits to equations (3) and (4) (Methods), respectively. Inset:  $G_{exc}f$  relationships for NMDAR with and without AMPAR STD (circles and squares, respectively). **c**, Average input–output relationships for AMPAR + NMDAR with and without AMPAR STD and tonic inhibition. Lines are Hill fits (equation (5)) and error bars are  $\pm$  s.e.m. **d**, Gain (green) and offset (orange) changes due to STD ( $\pm$ STD) and tonic inhibition ( $\pm$ inh) from fits in **c**.

mechanisms, such as AMPAR activation by means of spillover<sup>23</sup>. Increasing the level of STD increased the inhibition-mediated gain reduction (Supplementary Fig. 2c, d). Conversely, increasing the level of tonic inhibition increased the size of the gain reduction at all levels of STD. We also observed gain modulation with phasic inhibitory conductances, which are widespread in the central nervous system (Supplementary Fig. 3), confirming that STD-mediated gain modulation operates effectively with both phasic and tonic inhibition.

NMDA (*N*-methyl-D-aspartate) receptors (NMDARs) contribute to transmission at many central synapses and show a nonlinear voltage dependence. To examine experimentally how this synaptic component interacts with STD-based gain modulation, we measured the NMDAR component during Poisson stimulation of a single MF input and added it to the AMPAR conductance trains from the same GCs (Fig. 3a). The  $G_{exc}f$  relationships for the combined AMPAR and NMDAR components (Fig. 3b) were similar in shape to the AMPAR-only cases with and without STD (Fig. 2b), because the relationship between the mean NMDAR conductance and MF frequency was approximately linear (Fig. 3b, inset, and Supplementary Fig. 4). In the absence of AMPAR STD, 500 pS inhibition produced a slightly smaller gain reduction in the GC input–output relationship (Fig. 3c, d, 7.1%) than the AMPAR component alone (Fig. 1d, e, 12.6%), as predicted for noise-based gain modulation<sup>24</sup>. However, a robust inhibition-mediated gain reduction was observed with the depressing AMPAR component (Fig. 3d, 33.1%). These results show that synaptic activation of NMDARs in adult GCs, which contain the NR2C subunit<sup>25</sup>, is approximately linear with frequency and that this has little effect on STD-based gain modulation.

*In vivo* recordings show that finger extension<sup>20</sup> and facial stimulation<sup>19</sup> can produce high-frequency bursts of MF firing. To examine whether STD-mediated gain modulation can operate under such conditions, we recorded from GCs while stimulating individual MFs with high-frequency bursts to mimic activity *in vivo*<sup>19,20</sup>. This induced bursts of mixed AMPAR–NMDAR EPSCs under voltage-clamp, confirming reliable MF activation (Fig. 4a). In current-clamp, this produced GC firing from a potential of  $-75$  mV (Fig. 4b), as observed *in vivo*<sup>19</sup>. Firing rate was measured from the fourth stimulus to allow

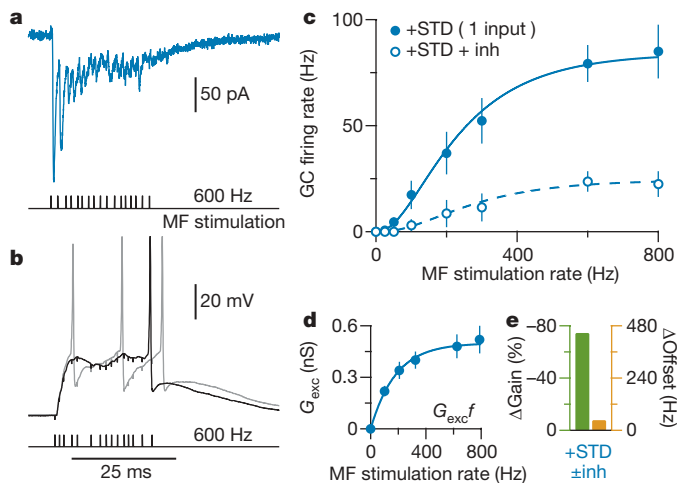


**Figure 4 | Gain modulation during broad bandwidth single mossy fibre stimulation.** **a**, Mixed AMPAR + NMDAR EPSCs in GCs during single MF, Poisson-burst-like stimulation (black ticks) at  $-75$  mV. Stimulus artefacts were subtracted. **b**, Voltage responses to burst-like MF stimulation with and without tonic inhibition (black and grey, respectively;  $G_{inh} = 500$  pS) injected by means of dynamic clamp. The black horizontal bar indicates the firing rate measurement window.  $V_{rest} = -74$  mV. **c**, Average GC input–output relationship with and without inhibition for single MF stimulation ( $n = 7$ ) with error bars ( $\pm$  s.e.m.) and Hill fits (equation (5)). **d**, Mean relationship between time-averaged conductance ( $G_{exc}$ ) and MF stimulation rate ( $f$ ). The blue line is an exponential fit (equation (4)). **e**, Gain (green) and offset (orange) changes due to inhibition ( $\pm inh$ ) computed from fits in **c**.

time for EPSC depression to occur<sup>21</sup>. A 500 pS tonic inhibitory conductance reduced firing (Fig. 4b) and produced a robust reduction in neuronal gain (Fig. 4c) that was twofold larger than for the four-fibre excitation (Figs 3d and 4e). The powerful nonlinearity between  $G_{exc}$  and  $f$  (Fig. 4d), combined with a purely additive shift in the  $FG_{exc}$  relationship, accounted for most of the inhibition-mediated gain change (Supplementary Fig. 5), confirming that it was mediated predominantly by STD.

Several factors complicate the implementation of multiplicative operations in neurons with extensive dendritic trees. The large voltage fluctuations required for noise-based gain modulation<sup>3,13,16,17</sup> are difficult to achieve with many inputs and heavy dendritic filtering, without precisely balanced excitation and inhibition<sup>3</sup>. Moreover, multiplication by means of nonlinear dendritic integration<sup>26</sup> or a combination of noise and dendritic saturation<sup>17</sup> requires spatially localized activation of synapses on a single dendritic branch, but these are usually distributed over the tree, making linear synaptic integration more likely<sup>26</sup>. To test whether the STD-mediated gain modulation can operate effectively in more complex neurons than GCs, we simulated synaptic integration in a neocortical layer 5 neuron model<sup>27</sup> with hundreds of synaptic inputs, randomly distributed over the

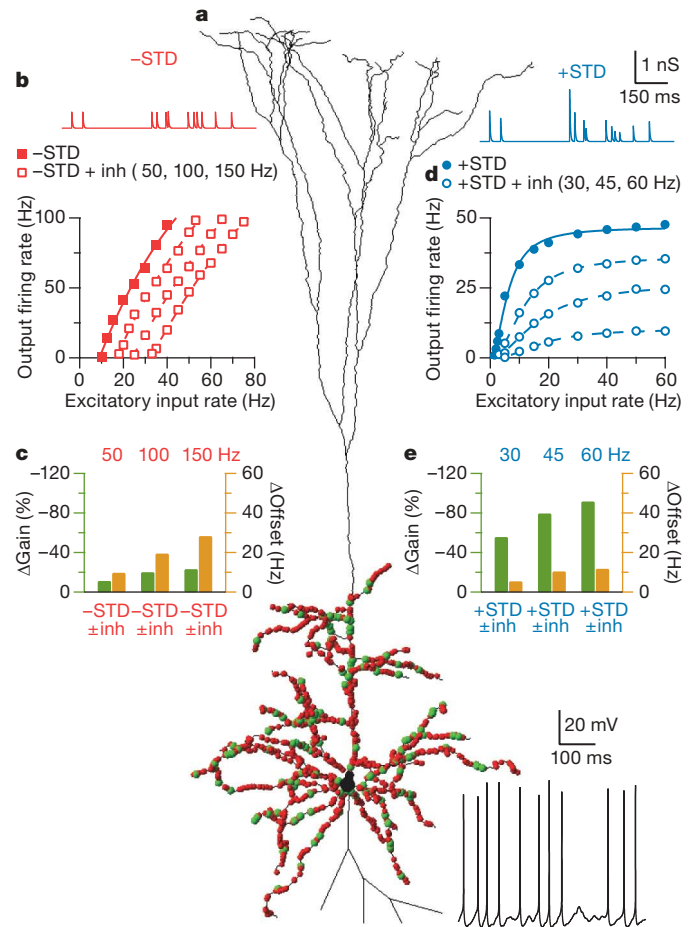


**Figure 5 | Multiplicative gain modulation in a cortical layer 5 pyramidal neuron model.** **a**, Layer 5 neuron model with location of excitatory (red circles) and inhibitory (green) synaptic contacts. Bottom: black trace shows spiking during synaptic excitation and inhibition. **b**, Top: conductance train for non-depressing unitary excitatory synaptic input. Bottom: input–output relationship for non-depressing synaptic excitation ( $-STD$ , red) for control conditions (solid symbols) and various rates of synaptic inhibition (open symbols) together with Hill fits (equation (5), Methods). **c**, Gain (green) and offset (orange) changes due to different inhibition rates ( $\pm inh$ ) in the absence of STD from fits in **b**. **d**, As for **b**, but for depressing synaptic excitation ( $+STD$ , blue) together with Hill fits. **e**, As for **c**, but for depressing synaptic excitation ( $+STD$ ) from fits in **d**.

basolateral dendritic tree (Fig. 5a and Methods). These simulations show that inhibitory synaptic input can act as a powerful modulator of neuronal gain when excitation is mediated by depressing synapses and yet perform a largely additive operation when it is absent (Fig. 5b–e). These results indicate that multiplicative operations are possible in cells with large dendritic arbors under conditions of linear integration when excitation is mediated by depressing synapses.

*In vivo*, MF–GC synapses typically operate at high frequencies<sup>20</sup>, where STD is pronounced<sup>19</sup>, although low-frequency vestibular inputs are a notable exception, where STD is absent and linear transmission is preserved<sup>28</sup>. At 100 Hz, STD is mediated predominantly by AMPAR desensitization<sup>21</sup>. AMPARs can therefore act as nonlinear ‘molecular amplifiers’ that contribute to single-cell computation. Although vesicle replenishment is rapid at MF release sites<sup>21</sup>, it will become limiting at higher frequencies and presynaptic STD will dominate. Presynaptic STD has a range of frequency dependencies across central synapses and can be modulated by long-term plasticity<sup>29</sup>, potentially allowing gain modulation to be matched to the operational frequency of the inputs.

Multiplication of driving and modulatory input conductance is most effective when synaptic depression has reached steady state. Because EPSC depression occurs rapidly in GCs ( $\tau_{\text{onset}} = 1.5$  pulses)<sup>21</sup>, gain modulation will only require a 4–75-ms settling time ( $2\tau_{\text{onset}}/\text{frequency}$ ; 40–800 Hz), but at cortical synapses where STD occurs at lower frequencies gain modulation will be slower. STD-mediated gain modulation allows a modulatory conductance to scale a neuron’s sensitivity to all of its driving inputs. This is distinct from the transient synaptic responses to changes in input rate, which allows signalling independent of absolute rate<sup>30</sup>. STD can therefore perform distinct multiplicative operations on different time scales: transient enhancement of the gain of dynamically changing inputs before STD has developed, and multiplication of all driving and modulatory inputs once depression has occurred.

Our findings show that the mathematical operation performed by a modulatory input on a particular set of driving inputs depends on their STD characteristics. This could allow input-configuration-specific, and thus context-dependent, computation at the level of a single neuron. The widespread incidence of STD, its compatibility with linear synaptic integration and the lack of dependence on synaptic noise indicate that this cellular mechanism for gain modulation could be used to multiply inputs together in many different neuronal types in the brain.

## METHODS SUMMARY

Whole-cell recordings were made from GCs at  $35.3 \pm 0.1$  °C ( $n = 62$ ) in rat cerebellar slices (postnatal day 30–40). EPSC trains for conductance clamp were recorded during stimulation of a single MF input at random Poisson intervals (mean rate  $f = 6$ –138 Hz). The NMDAR EPSC component was isolated by recording in  $5 \mu\text{M}$  2,3-dioxo-6-nitro-1,2,3,4-tetrahydrobenzo[f]quinoxaline-7-sulphonamide (NBQX). The AMPAR EPSC component was obtained by subtracting control and NBQX recordings. Conductance trains at each frequency were constructed by averaging ten responses, subtracting stimulus artefacts, dividing by the driving force, and averaging responses from four different GCs. AMPAR, NMDAR and tonic GABA conductances with reversal potentials of 0 mV, 0 mV and  $-75$  mV, respectively, were injected into GCs using a dynamic-clamp amplifier. Inhibition was blocked with  $10 \mu\text{M}$  SR95531. Direct activation of GC firing was achieved with single MF excitation using a 15-pulse Poisson stimulation (25–800 Hz). To minimize the effects of any time-dependent changes in excitability, MF excitation was randomized, control and tonic inhibition measurements interleaved, and experiments were carried out within 15 min of obtaining intracellular access to the GC. The cortical layer 5 neuron model<sup>27</sup> was connected to 400 excitatory neurons and 30 inhibitory neurons using neuroConstruct (<http://www.NeuroConstruct.org>) and run on the NEURON simulator (<http://www.neuron.yale.edu>). Data are presented as mean  $\pm$  s.e.m.

**Full Methods** and any associated references are available in the online version of the paper at [www.nature.com/nature](http://www.nature.com/nature).

Received 18 July; accepted 30 October 2008.

Published online 14 January 2009.

1. Koch, C. *Biophysics of Computation: Information Processing in Single Neurons* 552 (Oxford Univ. Press, 1999).

2. Holt, G. R. & Koch, C. Shunting inhibition does not have a divisive effect on firing rates. *Neural Comput.* **9**, 1001–1013 (1997).
3. Chance, F. S., Abbott, L. F. & Reyes, A. D. Gain modulation from background synaptic input. *Neuron* **35**, 773–782 (2002).
4. Anderson, J. S., Lampl, I., Gillespie, D. C. & Ferster, D. The contribution of noise to contrast invariance of orientation tuning in cat visual cortex. *Science* **290**, 1968–1972 (2000).
5. Treue, S. & Martinez Trujillo, J. C. Feature-based attention influences motion processing gain in macaque visual cortex. *Nature* **399**, 575–579 (1999).
6. Tovee, M. J., Rolls, E. T. & Azzopardi, P. Translation invariance in the responses to faces of single neurons in the temporal visual cortical areas of the alert macaque. *J. Neurophysiol.* **72**, 1049–1060 (1994).
7. Ingham, N. J. & McAlpine, D. GABAergic inhibition controls neural gain in inferior colliculus neurons sensitive to interaural time differences. *J. Neurosci.* **25**, 6187–6198 (2005).
8. Brothchie, P. R., Andersen, R. A., Snyder, L. H. & Goodman, S. J. Head position signals used by parietal neurons to encode locations of visual stimuli. *Nature* **375**, 232–235 (1995).
9. Yakusheva, T. A. et al. Purkinje cells in posterior cerebellar vermis encode motion in an inertial reference frame. *Neuron* **54**, 973–985 (2007).
10. Salinas, E. & Abbott, L. F. Transfer of coded information from sensory to motor networks. *J. Neurosci.* **15**, 6461–6474 (1995).
11. Pouget, A. & Sejnowski, T. J. Spatial transformations in the parietal cortex using basis functions. *J. Cogn. Neurosci.* **9**, 222–237 (1997).
12. Hansel, D. & van Vreeswijk, C. How noise contributes to contrast invariance of orientation tuning in cat visual cortex. *J. Neurosci.* **22**, 5118–5128 (2002).
13. Mitchell, S. J. & Silver, R. A. Shunting inhibition modulates neuronal gain during synaptic excitation. *Neuron* **38**, 433–445 (2003).
14. Gabbiani, F., Krapp, H. G., Koch, C. & Laurent, G. Multiplicative computation in a visual neuron sensitive to looming. *Nature* **420**, 320–324 (2002).
15. Tiesinga, P. H., Jose, J. V. & Sejnowski, T. J. Comparison of current-driven and conductance-driven neocortical model neurons with Hodgkin–Huxley voltage-gated channels. *Phys. Rev. E* **62**, 8413–8419 (2000).
16. Murphy, B. K. & Miller, K. D. Multiplicative gain changes are induced by excitation or inhibition alone. *J. Neurosci.* **23**, 10040–10051 (2003).
17. Prescott, S. A. & De Koninck, Y. Gain control of firing rate by shunting inhibition: roles of synaptic noise and dendritic saturation. *Proc. Natl Acad. Sci. USA* **100**, 2076–2081 (2003).
18. Fellous, J. M., Rudolph, M., Destexhe, A. & Sejnowski, T. J. Synaptic background noise controls the input/output characteristics of single cells in an *in vitro* model of *in vivo* activity. *Neuroscience* **122**, 811–829 (2003).
19. Rancz, E. A. et al. High-fidelity transmission of sensory information by single cerebellar mossy fibre boutons. *Nature* **450**, 1245–1248 (2007).
20. van Kan, P. L., Gibson, A. R. & Houk, J. C. Movement-related inputs to intermediate cerebellum of the monkey. *J. Neurophysiol.* **69**, 74–94 (1993).
21. Saviane, C. & Silver, R. A. Fast vesicle reloading and a large pool sustain high bandwidth transmission at a central synapse. *Nature* **439**, 983–987 (2006).
22. Semyanov, A., Walker, M. C., Kullmann, D. M. & Silver, R. A. Tonic active GABA A receptors: modulating gain and maintaining the tone. *Trends Neurosci.* **27**, 262–269 (2004).
23. DiGregorio, D. A., Nusser, Z. & Silver, R. A. Spillover of glutamate onto synaptic AMPA receptors enhances fast transmission at a cerebellar synapse. *Neuron* **35**, 521–533 (2002).
24. Berends, M., Maex, R. & De Schutter, E. The effect of NMDA receptors on gain modulation. *Neural Comput.* **17**, 2531–2547 (2005).
25. Cathala, L., Misra, C. & Cull-Candy, S. Developmental profile of the changing properties of NMDA receptors at cerebellar mossy fiber–granule cell synapses. *J. Neurosci.* **20**, 5899–5905 (2000).
26. London, M. & Hausser, M. Dendritic computation. *Annu. Rev. Neurosci.* **28**, 503–532 (2005).
27. Kole, M. H. et al. Action potential generation requires a high sodium channel density in the axon initial segment. *Nature Neurosci.* **11**, 178–186 (2008).
28. Arenz, A., Silver, R. A., Schaefer, A. T. & Margrie, T. W. The contribution of single synapses to sensory representation *in vivo*. *Science* **321**, 977–980 (2008).
29. Markram, H. & Tsodyks, M. Redistribution of synaptic efficacy between neocortical pyramidal neurons. *Nature* **382**, 807–810 (1996).
30. Abbott, L. F., Varela, J. A., Sen, K. & Nelson, S. B. Synaptic depression and cortical gain control. *Science* **275**, 220–224 (1997).

**Supplementary Information** is linked to the online version of the paper at [www.nature.com/nature](http://www.nature.com/nature).

**Acknowledgements** This was supported by the Wellcome Trust, MRC (G0400598) and EU (EUSynapse, LSHM-CT-2005-019055). R.A.S. is in receipt of a Wellcome Senior Research Fellowship. We thank P. Gleeson for help with neuroConstruct, D. Ward and R. Kanichay for their experimental support, D. Digregorio and P. Kirkby for discussions, and A. Arenz, D. Attwell, G. Billings, E. Chaigneau, D. DiGregorio, M. Farrant, F. Minneci and K. Vervaeke for their comments on the manuscript.

**Author Information** Reprints and permissions information is available at [www.nature.com/reprints](http://www.nature.com/reprints). Correspondence and requests for materials should be addressed to R.A.S. ([a.silver@ucl.ac.uk](mailto:a.silver@ucl.ac.uk)).

## METHODS

Parasagittal slices (200–250  $\mu\text{m}$ ) of the cerebellar vermis were prepared<sup>23,31,32</sup> from Sprague-Dawley rats (P30–40) in ACSF solution containing (in mM) 125 NaCl, 2.5 KCl, 26  $\text{NaHCO}_3$ , 1.25  $\text{NaH}_2\text{PO}_4$ , 2  $\text{CaCl}_2$ , 1  $\text{MgCl}_2$ , 25 glucose and 0.5 ascorbic acid (pH 7.4 when bubbled with 95%  $\text{O}_2$  and 5%  $\text{CO}_2$ ), or in a low-sodium sucrose solution containing (in mM) 85 NaCl, 2.5 KCl, 26  $\text{NaHCO}_3$ , 1.25  $\text{NaH}_2\text{PO}_4$ , 0.5  $\text{CaCl}_2$ , 4  $\text{MgCl}_2$ , 25 glucose, 63.4 sucrose and 0.5 ascorbic acid. In some preparations 1 mM kynurenic acid or 10  $\mu\text{M}$  D-(–)-2-amino-5-phosphonopentanoic acid (D-AP5) was added to block glutamate receptors. After ~30 min incubation at 32 °C, slices were transferred to ACSF solution at room temperature (~20 °C). Whole-cell recordings with a series resistance of  $27.9 \pm 1.3 \text{ M}\Omega$  ( $n = 62$ ) were made with an Axopatch 200B amplifier, filtered at 7–10 kHz, and digitized at 33–100 kHz using an InstruTech ITC-18 board and Axograph or NeuroMatic software (<http://www.neuromatic.thinkrandom.com>). GCs had a cell capacitance of  $3.2 \pm 0.1 \text{ pF}$  ( $n = 62$ ) and a resting membrane potential of  $-78.5 \pm 0.9 \text{ mV}$  ( $n = 52$ ). Data were analysed using NeuroMatic within the Igor Pro environment (WaveMetrics).

**Synaptic conductance trains and dynamic-clamp.** Whole-cell recordings were made from GCs perfused with ACSF containing 0.3  $\mu\text{M}$  strychnine and 10  $\mu\text{M}$  SR95531 (Gabazine) to block inhibitory receptors, and 3  $\mu\text{M}$  glycine to ensure NMDAR activation. Recordings of EPSC trains to be used for dynamic-clamp were made at  $-54 \text{ mV}$  or  $-60 \text{ mV}$ , using fire-polished borosilicate micropipettes containing (in mM) 110  $\text{KmeSO}_3$ , 4 NaCl, 1.78  $\text{CaCl}_2$ , 0.3 Na-GTP, 4 Mg-ATP, 40 HEPES and 5 EGTA (pH 7.3), or in some cases 90 CsCl, 10 NaCl, 1.78  $\text{CaCl}_2$ , 0.3 Na-GTP, 4 Mg-ATP, 40 HEPES, 5 EGTA and 5 TEA (pH 7.3). EPSCs were evoked by extracellular stimulation of a single MF input<sup>31</sup> using Poisson stimulation trains (PSTs) of 250–2,500 ms duration with a 1-ms minimum refractory interval. Ten repetitions of four statistically different PSTs were recorded from each MF–GC synapse at each frequency. Stimulus artefacts were removed by convolving a single stimulus artefact with the PST, and subtracting the resulting waveform from the averaged data. Synaptic current trains were converted to conductance trains by dividing by the holding potential, after correcting for the liquid junction potential<sup>13,32</sup>. Conductance trains with the same statistics from four different GCs were aligned and averaged, and had a mean conductance close to the population mean<sup>23,32</sup>. To create non-depressing AMPAR conductance trains, the first AMPAR response of each train was fit with the following multiple-exponential function:

$$G(t) = (1 - e^{-t/\tau_1})^n [a_1 e^{-t/\tau_{d1}} + a_2 e^{-t/\tau_{d2}} + a_3 e^{-t/\tau_{d3}}] \quad (1)$$

Where  $e$  is the base of the natural logarithm,  $\tau_i$  and  $\tau_{d1-3}$  are the time constants of the rising and decaying components, respectively,  $a_{1-3}$  are the amplitude components and  $t$  is time. The resulting fit was then convolved with the given PST to create a non-depressing train (Fig. 1b, red trace).

**Dynamic-clamp recordings and spike analysis.** Slices were perfused with ACSF containing 10  $\mu\text{M}$  SR95531 to block tonic GABA currents. Dynamic-clamp recordings<sup>33,34</sup> were made from GCs using fire-polished borosilicate micropipettes containing (in mM) 114  $\text{KmeSO}_3$ , 6 NaOH, 3  $\text{MgCl}_2$ , 0.02  $\text{CaCl}_2$ , 0.3 Na-GTP, 4 Na-ATP, 40 HEPES and 0.15 BAPTA (pH 7.3). A liquid junction potential of +6.3 mV ( $n = 5$ ) was corrected before gaining whole-cell access. During recordings, the resting membrane potential ( $V_{\text{rest}}$ ) was maintained near  $-80 \text{ mV}$  using small amounts of holding current. Conductance trains were injected with a three-channel SM1 amplifier (Cambridge Conductance). Because GCs receive an average of four MF inputs, and often require more than one input to fire<sup>35,36</sup>, AMPAR conductance trains (and NMDAR conductance trains) from four statistically different PSTs were summed together at each input frequency ( $f$ ) before injection into GCs by means of dynamic-clamp as described below.

Unlike the AMPAR component, which follows a simple linear Ohmic relationship with voltage, the NMDAR component introduced by the SM1 amplifier has a Boltzmann-like nonlinearity that mimics the voltage-dependent  $\text{Mg}^{2+}$  block of the NMDA conductance measured in GCs (Supplementary Fig. 4). This nonlinearity introduced by the SM1 amplifier scaled the NMDAR conductance waveforms so that the final peak value, after leaving the SM1 amplifier, matched that of GCs, as described by the following Boltzmann function:

$$G_{\text{exc}}(V) = \frac{G_{\text{max}}}{1 + e^{-(V - V_{0.5})/k}} \quad (2)$$

where  $G_{\text{max}} = 367.9 \text{ pS}$ ,  $V_{0.5} = -12.8 \text{ mV}$  and  $k = 22.4 \text{ mV}$  ( $n = 6$  cells; curve fit to data in Supplementary Fig. 4a). During the experiments, conductance trains at various  $f$  were injected in a random order, and conditions with and without tonic inhibition ( $G_{\text{inh}} = 500 \text{ pS}$ ; steps began 10 ms before onset of the synaptic input) were presented consecutively at each  $f$ . Some GCs were excluded because their output spike rate was too low or absent in the presence of STD and tonic inhibition (13 out of 36 cells), preventing an accurate measurement of a gain change. This will tend to underestimate the gain change we report. Cells were also

discarded if the heights of their action potentials changed more than 10% during the experiment (3 out of 36 cells). For dynamic-clamp experiments, GC output firing rate ( $F$ ) was calculated from 100 ms after the onset to the end of the stimulus train. Action potentials were detected using a threshold-level detection set at 0 mV.

**Granule cell excitation with mossy fibre stimulation.** GCs were directly activated by stimulating single MF inputs with burst PSTs ( $f = 25\text{--}800 \text{ Hz}$ ; 1 ms minimum refractory interval) to mimic *in vivo* MF activity<sup>19,20</sup>. Bursts lasted for a period  $T = 15/f$  seconds, consisting of approximately 15 stimuli. Average conductance and output spike rate were computed over the same period  $T$ , but starting from the time of the fourth stimulus, when STD reached approximate steady-state levels<sup>21</sup>. Recording conditions were the same as those described for the dynamic-clamp recordings, except  $V_{\text{rest}}$  was maintained at  $-75 \text{ mV}$  rather than  $-80 \text{ mV}$  because most GCs (69%;  $n = 22$  of 32) either did not fire action potentials when stimulated from their resting potential or did not produce enough output spikes to compute an input–output relationship in the range 25–800 Hz. Tonic inhibition was applied with dynamic-clamp ( $G_{\text{inh}} = 500 \text{ pS}$ ; steps began 75 ms before onset of the synaptic stimulation) and was alternated with control conditions at each  $f$ .

**Data analysis.** Plots of average excitatory conductance ( $G_{\text{exc}}$ ) versus MF input rate  $f$  ( $G_{\text{exc}}f$  relationships; Figs 2b and 3b) were fit with a linear equation for AMPAR conductances without STD:

$$G_{\text{exc}}(f) = mf \quad (3)$$

and an exponential function for AMPAR conductances with STD:

$$G_{\text{exc}}(f) = m\lambda[1 - e^{-f/\lambda}] \quad (4)$$

where  $\lambda$  is a frequency constant and  $m$  is a shared slope factor. At low frequencies ( $f \ll \lambda$ ), these two equations are approximately equal. Plots of GC firing rate  $F$  versus  $G_{\text{exc}}$  ( $FG_{\text{exc}}$  relationships) were well described by a Hill equation of the form:

$$F(G_{\text{exc}}) = \frac{F_{\text{max}}}{1 + (G_{\text{exc}}50/G_{\text{exc}})^n} + F_0 \quad (5)$$

where  $n$  is the exponent factor,  $F_0$  is the firing rate offset,  $F_{\text{max}}$  is the maximum firing rate and  $G_{\text{exc}}50$  is the value of  $G_{\text{exc}}$  at which  $F$  reaches half maximum. For  $n = 1$  the relationship is a simple saturating function (Fig. 2d, inset) and for  $n > 1$  the relationship is sigmoidal (Fig. 2c). Input–output relationships (Figs 1d, 3c and 4c) were also fit with equation (5), but with  $G_{\text{exc}}(f)$  substituted for  $G_{\text{exc}}$ , where  $G_{\text{exc}}(f)$  was described by equation (3) for the AMPAR component without STD, and equation (4) for STD ( $\lambda$  and  $m$  held constant during the fits). Similar results were obtained by fitting a simple Hill function (equation (5)), with  $f$  substituted for  $G_{\text{exc}}$ , but the STD input–output data were less well described by this function than when equations (4) and (5) were combined, as theoretically predicted. Fits of the input–output relationships with and without inhibition were compared using the  $F$ -ratio for the separate and combined data sets. All fits were significantly different ( $P < 0.05$ ). The gain was calculated from the average slope ( $F'$ ) of the fits between 5% and 75% its maximum value. An upper limit of 75% was used so that all computations of  $F'$  were limited to the range of our experimental data. Changes in gain ( $\Delta\text{Gain}$ ) were computed as follows:

$$\Delta\text{Gain} = \left( \frac{F'_{+a} - F'_{-a}}{F'_{-a}} \right) \quad (6)$$

where  $+a$  and  $-a$  denote conditions with and without inhibition ( $\pm\text{inh}$ ) or with and without STD ( $\pm\text{STD}$ ). Additive offset shifts ( $\Delta\text{Offset}$ ) were defined as the difference between the half-maximum frequencies of the fits for the two conditions  $+a$  and  $-a$ .

**Neuronal models.** A GC-like conductance-based integrate-and-fire model was implemented in the NEURON simulation environment<sup>37</sup> and was described by the following equation:

$$-C_m \frac{dV}{dt} = \frac{(V - E_L)}{R_m} + D(t)G_{\text{AMPA}}(V - E_{\text{AMPA}}) + G_{\text{GABA}}(V - E_{\text{GABA}}) \quad (7)$$

where  $C_m = 3.1 \text{ pF}$ , the reversal potentials for the leak  $E_L = -75 \text{ mV}$ , AMPARs  $E_{\text{AMPA}} = 0 \text{ mV}$  and GABA<sub>A</sub>s  $E_{\text{GABA}} = -75 \text{ mV}$ , and a membrane resistance  $R_m = 2.6 \text{ G}\Omega$ <sup>13,32</sup>. Spikes were generated when the model reached a threshold of  $-49 \text{ mV}$ , at which time the voltage was set to  $10 \text{ mV}$  for one integration time step, and then clamped to  $-75 \text{ mV}$  for a refractory period of 2.5 ms. The AMPAR conductance was described by equation (1), using the following values computed from fits to our GC AMPAR conductance data:  $n = 11$ ,  $\tau_1 = 0.10 \text{ ms}$ ,  $a_1 = 2.23 \text{ nS}$ ,  $\tau_{d1} = 0.45 \text{ ms}$ ,  $a_2 = 0.29 \text{ nS}$ ,  $\tau_{d2} = 2.88 \text{ ms}$ ,  $a_3 = 0.08 \text{ nS}$  and  $\tau_{d3} = 21.67 \text{ ms}$ . For simulations with STD, whenever the integrate-and-fire model received an excitatory input, the amplitude of the postsynaptic AMPAR

response was multiplied by a scale factor  $\delta$  ( $D \rightarrow D\delta$ )<sup>38</sup>. Between inputs,  $D$  recovered exponentially back to its initial value of 1.0 with a time constant  $\tau_D = 40$  ms. For simulations with phasic inhibitory input (Supplementary Fig. 3) the synaptic GABAR conductance was described by equation (1) using the following values:  $n = 8.34$ ,  $\tau_r = 0.14$  ms,  $a_1 = 53.02$ ,  $\tau_{d1} = 0.05$  ms,  $a_2 = 0.53$ ,  $\tau_{d2} = 6.90$  ms and  $a_3 = 0$  (R. Kanichay and R.A.S., unpublished data). The peak conductance was set to 663 pS to give a time-averaged conductance of 500 pS at 100 Hz. Mean input rates were 50–150 Hz.

A model of a cortical layer 5 neuron<sup>27</sup> was synaptically connected to 400 excitatory neurons and 30 inhibitory neurons using neuroConstruct<sup>39</sup> (<http://www.NeuroConstruct.org>) and the code was automatically generated for the NEURON simulator<sup>37</sup>. Each excitatory connection cell had three synaptic contacts (to model six contacts with intermediate release probability)<sup>40</sup> and inhibitory connections had five synaptic contacts (to model ten synaptic inputs)<sup>41</sup>. Both input types were distributed randomly over the basolateral dendritic tree and soma to mimic layer 5–layer 5 connectivity. Excitatory synaptic inputs had a conductance time course described by two exponential functions ( $\tau_{\text{rise}} = 0.3$  ms,  $\tau_{\text{decay}} = 3$  ms) and a peak conductance of 3 nS<sup>40</sup> (that is, 1 nS at each of the three synaptic contacts). Each presynaptic excitatory neuron was driven to fire an independent Poisson spike train (1–70 Hz) and the synaptic conductance was scaled by the level of STD, which was implemented as described previously using experimentally measured values for layer 5 pyramidal cell connections (where the fraction of synaptic resource used,  $U_{\text{se}}$ , was equal to 0.5, and the time constants of inactivation and recovery were  $\tau_{\text{inact}} = 3$  ms and  $\tau_{\text{recov}} = 500$  ms, respectively)<sup>42</sup>. Inhibitory synaptic inputs had fixed conductances with a dual exponential time course ( $\tau_{\text{rise}} = 0.3$  ms,  $\tau_{\text{decay}} = 10$  ms) and a peak conductance of 3.5 nS<sup>41</sup>. Presynaptic inhibitory neurons were driven with independent Poisson trains with mean rates 30–150 Hz. Reversal potentials for excitatory and inhibitory conductances were 0 mV and  $-75$  mV, respectively. Because the excitatory drive for non-depressing synapses was much higher than the more physiological depressing inputs, we carried out simulations with two different synaptic conductances (3 nS and 0.5 nS) for the non-STD case. 50 Hz inhibition produced a similar gain change for the two conductances ( $-11.7\%$  and  $-10.9\%$ , respectively), but the larger conductance gave a bigger gain change at 150 Hz as expected for noise-based gain modulation ( $-28.6\%$  versus  $-22.9\%$ ). The 0.5 nS value was chosen for comparison because the excitatory input drive (0–70 Hz) better matched that of the STD case (0–60 Hz; Fig. 5b, d) than for 3 nS inputs, which saturated firing at input rates of only 12 Hz. Output firing rate was measured at steady state. Input–output relationships were fit with a simple Hill function similar to equation (5), but with input frequency ( $f$ ) substituted for  $G_{\text{exc}}$ , owing to difficulty in defining the effective  $G_{\text{exc}}$  for a distributed input.  $\Delta\text{Gain}$  and  $\Delta\text{Offset}$  were calculated from the fits as above, except for the  $-STD$  simulations, which showed little saturation of firing rate. In this case,  $\Delta\text{Gain}$  and

$\Delta\text{Offset}$  were calculated assuming a maximum rate of 100 Hz. Because the model<sup>27</sup> had an input resistance in the absence of synaptic input (11.5 M $\Omega$ ) at the low end of that measured experimentally 9–123 M $\Omega$  (mean 36 M $\Omega$ )<sup>43</sup>, we repeated the simulations with a different model<sup>44</sup> with a high-input resistance (79 M $\Omega$ ), which we modified to fire repetitively. We obtained similar results for the effects of inhibitory synaptic input on the input–output relationship in the presence and absence of STD in the excitatory input (data not shown), although fewer presynaptic cells (100 excitatory and 20 inhibitory) were required to drive the model over a similar range of frequencies.

31. Silver, R. A., Cull-Candy, S. G. & Takahashi, T. Non-NMDA glutamate receptor occupancy and open probability at a rat cerebellar synapse with single and multiple release sites. *J. Physiol. (Lond.)* **494**, 231–250 (1996).
32. Cathala, L., Brickley, S., Cull-Candy, S. & Farrant, M. Maturation of EPSCs and intrinsic membrane properties enhances precision at a cerebellar synapse. *J. Neurosci.* **23**, 6074–6085 (2003).
33. Robinson, H. P. & Kawai, N. Injection of digitally synthesized synaptic conductance transients to measure the integrative properties of neurons. *J. Neurosci. Methods* **49**, 157–165 (1993).
34. Sharp, A. A., O’Neil, M. B., Abbott, L. F. & Marder, E. Dynamic clamp: computer-generated conductances in real neurons. *J. Neurophysiol.* **69**, 992–995 (1993).
35. D’Angelo, E., De Filippi, G., Rossi, P. & Taglietti, V. Synaptic excitation of individual rat cerebellar granule cells *in situ*: evidence for the role of NMDA receptors. *J. Physiol. (Lond.)* **482**, 397–413 (1995).
36. Jorntell, H. & Ekerot, C. F. Properties of somatosensory synaptic integration in cerebellar granule cells *in vivo*. *J. Neurosci.* **26**, 11786–11797 (2006).
37. Hines, M. L. & Carnevale, N. T. The NEURON simulation environment. *Neural Comput.* **9**, 1179–1209 (1997).
38. Varela, J. A. *et al.* A quantitative description of short-term plasticity at excitatory synapses in layer 2/3 of rat primary visual cortex. *J. Neurosci.* **17**, 7926–7940 (1997).
39. Gleeson, P., Steuber, V. & Silver, R. A. neuroConstruct: a tool for modeling networks of neurons in 3D space. *Neuron* **54**, 219–235 (2007).
40. Markram, H., Lubke, J., Frotscher, M., Roth, A. & Sakmann, B. Physiology and anatomy of synaptic connections between thick tufted pyramidal neurones in the developing rat neocortex. *J. Physiol. (Lond.)* **500**, 409–440 (1997).
41. Gupta, A., Wang, Y. & Markram, H. Organizing principles for a diversity of GABAergic interneurons and synapses in the neocortex. *Science* **287**, 273–278 (2000).
42. Tsodyks, M. V. & Markram, H. The neural code between neocortical pyramidal neurons depends on neurotransmitter release probability. *Proc. Natl Acad. Sci. USA* **94**, 719–723 (1997); erratum **94**, 5495 (1997).
43. Schwindt, P. C., O’Brien, J. A. & Crill, W. E. Quantitative analysis of firing properties of pyramidal neurons from layer 5 of rat sensorimotor cortex. *J. Neurophysiol.* **77**, 2484–2498 (1997).
44. Mainen, Z. F., Joerges, J., Huguenard, J. R. & Sejnowski, T. J. A model of spike initiation in neocortical pyramidal neurons. *Neuron* **15**, 1427–1439 (1995).